RSC Advances

ROYAL SOCIETY OF CHEMISTRY

www.rsc.org/advances

Carbon Dots/NiAl-layered double hydroxide hybrid material: facile synthesis, intrinsic peroxidase-like catalytic activity and its application

Yali Guo, Xiaoyu Liu, Xudong Wang, Anam Iqbal, Chengduan Yang, Weisheng Liu, and Wenwu Qin *

[Oct 6, 2015]

Key Laboratory of Nonferrous Metal Chemistry and Resources Utilization of Gansu Province and State Key Laboratory of Applied Organic Chemistry, College of Chemistry and Chemical Engineering, Lanzhou University, Lanzhou 730000, P. R. China.

*To whom correspondence should be addressed. E-mail: W. Qin: qinww@lzu.edu.cn, Tel.: +86 -931-8912582; Fax: +86-931-8912582

Abstract

A novel carbon dots/NiAl-layered double hydroxide (C-dots/NiAl-LDH) hybrid material is successfully prepared through the electrostatically self-assembly of positively charged NiAl-LDH nanoplates (3.74 ± 0.3 mV) and negatively charged C-dots (-5.09 ± 0.5 mV). The morphology, structure, composition and fluorescence properties of the hybrid material are characterized by different techniques, such as transmission electron microscopy (TEM), X-ray diffraction (XRD), X-ray photoelectron spectroscopy (XPS), Fourier-transform infrared spectroscopy (FTIR), and fluorescence spectroscopy. Moreover, C-dots/NiAl-LDH exhibits intrinsic peroxidase-like activity, which shows enhanced catalytic activities compared with C-dots and NiAl-LDH. The hybrid material facilitates the electron transfer between 3, 3′, 5, 5′-tetramethylbenzidine (TMB) and H_2O_2, which oxidizes TMB to form a blue product. On the basis of the peroxidase-like activity of C-dots/NiAl-LDH, the hybrid material can employ to colorimetric detection of H_2O_2 with a lower detection limit of 0.11 μM. The hybrid material also exposes better stability than horseradish peroxidase (HRP) when they are exposed to solutions with different organic solvents and temperatures. The proposed method is successfully applied for the determination of H_2O_2 in milk samples.

1. Introduction

In recent years, artificial enzymes have received considerable attention due to their advantages over natural enzymes, such as design flexibility, excellent stability and tunable catalytic activity.[1] With the development of nanoscience and nanotechnology,

metal oxides (Fe_3O_4,[2] CuO,[3] MnO_2,[4] V_2O_5[5]), metal sulfides (FeS,[6] CuS,[7] MoS_2[8]), metal nanoparticles (NPs),[9-11] carbon nanomaterials[12-14] and other nanomaterials[15-16] have been exploited to serve as peroxidase mimetics. When compared with the corresponding single nanomaterial, hybrid materials tend to expose higher catalytic activity. Typically, CuS-graphene composites, [17] hemin–graphene hybrid nanosheets, [18] BSA–PtNPs, [19] carbon dots–Pt nanocomposites [20] have been reported with peroxidase-like activity. These hybrid materials exhibit enhanced catalytic activity due to the enlarged effective surface area and the synergic effect of each components. However, some of them are high cost, and their preparation process is complicated. Therefore, it is still necessary to design and fabricate new, low cost, and easily prepared hybrid materials with peroxidase-like activity.

Layered double hydroxides (LDHs) are a class of layered materials and composed of positively-charged brucite-like layers and interlayer anions, which have been widely employed in chemical sensing, supercapacitors, electrochemistry, magnetism and catalysis.[21-24] In particular, the layered structure, large surface area, good adsorption ability and anion exchange properties of LDHs make them potentially material as matrix for peroxidase mimetics .[25-26]

Carbon dots (C-dots) have gradually become a rising star, due to its robust chemical inertness, easy functionalization, supernal conductivity, low toxicity and good biocompatibility.[27-29] Recently, C-dots have been introduced into layered double hydroxides successfully, such as NiFe-LDH,[30] CoFe-LDH,[31] MgAl-LDH,[32] for various applications. Nevertheless, to the best of our knowledge, C-dots/LDH hybrid

material has not been used as peroxidase mimetics.

In this work, we report the fabrication of C-dots/NiAl-LDH hybrid material through a simple electrostatically self-assembly route. The morphology, structure, fluorescence properties and peroxidase-like activity of the hybrid material were systematically investigated. Meanwhile, we have tested the hybrid material as a novel peroxidase mimetic to offer a simple, sensitive and selective colorimetric method for H_2O_2 detection in milk simples.

2. Experimental section

2.1 Chemicals

Nickel(II) nitrate hexahydrate ($Ni(NO_3)_2$•$6H_2O$, Tianjin chemical reagent factory, ≥98%), Aluminum (III) nitrate nonahydrate ($Al(NO_3)_3$•$9H_2O$, Shanghai chemical reagent factory, ≥98%), Hydrogen Peroxide (H_2O_2, Sinopharm Chem. Reagent Co., Ltd. ⩾30 wt.%), Citric acid monohydrate (CA, ⩾99.5%), sodium hydroxide (NaOH, ⩾96%) and Sodium carbonate anhydrous (Na_2CO_3, ⩾99.8%) were purchased from Tianjin Guangfu Reagent Company. Horseradish peroxidase (HRP, 250 u/mg), 3, 3′, 5, 5′-tetramethylbenzidine (TMB, ⩾ 98%), o-phenylenediamine (OPD, ⩾ 98%), 2,2-azino-bis(3-ethylbenzothiazoline-6-sulfonic acid) (ABTS), 3,3'-Diaminobenzidine (DAB, ⩾98%), trichloroacetic acid (TCA) were purchased from Energy Chemical. Terephthalic acid (TA; ≥ 98.5 %) was purchased from Chengdu cologne chemical reagent factory. All reagents and solvents were of analytical grade and directly used without further purification and all aqueous solutions were prepared with Milli-Q water (18.2 MΩ cm).

2.2 Instrument

The morphology and microstructure of samples were analyzed by transmission electron microscopy (TEM) (JEM-2100) equipped with an energy-dispersive X-ray spectrometer (EDX). The samples were dispersed in ethanol and then dried on a holey carbon film Cu grid. The ζ-potentials of the NiAl-LDH and C-dots were determined on a Zetasizer 3000HS nanogranularity analyzer for three repeated measurements (Malvern Instruments, UK). XRD measurements were performed on a X-ray diffractometer (D/max-2400pc, Rigaku, Japan) using Cu Kα radiation (λ = 1.54178 Å), using an operating voltage and current of 40 kV and 60 mA, respectively. The 2θ range was from 10 to 90 in steps of 0.02^{o}. For XRD observations, the samples were dispersed in ethanol and then dried on a glass slide. X-ray photoelectron spectra (XPS) were measured on a PHI-550 spectrometer by using Mg Kα radiation (hν = 1253.6 eV) photoemission spectroscopy with a base vacuum operated at 300 W. The Fourier transform infrared spectroscopy (FTIR) spectra were measured on a Nicolet 360 FTIR spectrometer using the KBr pellet technique.

2.3 Steady-state UV-vis absorption and fluorescence spectroscopy

The absorbance of catalytic reaction processes were recorded on a UV-visible spectrometer (Cary 100) under experimental conditions. The steady-state excitation and emission spectra was obtained on a FLS920 spectrofluorometer. 3D spectra were collected with an excitation range of 300-500 nm and an emission range of 320-590 nm. Freshly prepared samples in 1 cm quartz cells were used to perform all UV-vis absorption and emission measurements.

Quantum yields were determined by an absolute method using an integrating sphere based upon that originally developed by de Mello[33] et al. Experiments were conducted on an FLS920 from Edinburgh Instruments.

2.4 Time-resolved fluorescence spectroscopy

Fluorescence lifetimes were measured on an Edinburgh Instruments FLS920 equipped with different light emitting diodes (excitation wavelength 330 nm), using the time-correlated single photon counting technique[34] in 2048 channels at room temperature. The sample concentrations were adjusted to optical densities at the excitation wavelength (330 nm) < 0.1. The monitored wavelengths were 420 nm, 440 nm, and 460 nm.

Histograms of the instrument response functions (using LUDOX scattering) and sample decays were recorded until they typically reached 5.0×10^3 counts in the peak channel. Obtained histograms were fitted as sums of the exponentials, using Gaussian-weighted nonlinear least squares fitting based on Marquardt–Levenberg minimization implemented in the software package of the instrument. The fitting parameters (decay times and pre-exponential factors) were determined by minimizing the reduced χ^2. An additional graphical method was used to judge the quality of the fit that included plots of surfaces (‘‘carpets’’) of the weighted residuals vs. channel number. All curve fittings presented here had χ^2 values < 1.1.

2.5 Preparation of NiAl–LDH

NiAl-LDH was prepared according to a reported method.[35] Typically, 10 mL of mixed alkali solution containing NaOH (0.08 M) and Na_2CO_3 (0.02 M) was prepared.

Subsequently, the solution was titrated with 10 ml of a salt solution of $Ni(NO_3)_2$ (0.03 M) and $Al(NO_3)_3$ (0.01 M) under vigorous stirring at room temperature. The pH value of the solution was adjusted to 10.5 by further titration with 0.08 M NaOH solution. The suspension was then aged at 60°C for 6 h. Finally, the obtained precipitate was washed with deionized water for three times and dried at 60°C for 12 h.

2.6 Synthesis of C-dots/NiAl-LDH

C-dots were prepared according to the previous report, [36-37] and the details were described in the Supporting Information (S1.1†). C-dots/NiAl-LDH hybrid material was prepared via a simple process. In brief, 5.0 mL C-dots aqueous suspension was mixed with 0.1 g prepared NiAl-LDH. The obtained suspension was kept vigorously stirring at room temperature for overnight. The crude product was isolated through centrifugation and washed with water. Finally, the pure product was dispersed in 100 mL double-distilled water for further use.

2.7 Peroxidase-like activity and kinetic analysis of the C-dots/NiAl-LDH

The peroxidase-like activity of the C-dots/NiAl-LDH was tested through the catalytic oxidation of 3, 3′, 5, 5′-tetramethylbenzidine (TMB) in the presence of H_2O_2. Typically, 50 μL TMB (8 mM), 20 μL H_2O_2 (30 wt. %) and 50 μL of colloidal C-dots/NiAl-LDH nanoparticles were added into 2 mL sodium acetate buffer solution (pH = 3.0) at 30°C. The reactions were carried out for 10 min and then monitored by observing the absorbance at 652 nm. Additionally, the apparent steady-state kinetic measurements were carried out under varying concentration of TMB at a fixed concentration of H_2O_2 or vice versa. The Michaelis–Menten constant was calculated

by using the Lineweaver–Burk plot: $1/V_0 = (K_m /V_m) (1/[S] +1/K_m)$, where V_0 is the initial velocity, V_m is the maximal reaction velocity, and [S] is the concentration of the substrate.

2.8 Detection of H_2O_2

In a typical process, the TMB solution (50 μL, 8 mM) and 20 μL H_2O_2 in various concentrations (0.2–500 μM) were added to 2 mL acetate buffer solution (pH = 3.0), then 50 μL of the catalyst was added into the mixture, and the UV -vis spectra were recorded after reaction for 10 min at 30 ℃.

For H_2O_2 determination in aseptic milk samples, the samples were firstly precipitated by 20% (w/w) trichloroacetic acid (TCA). Then, the mixture was filtered, and the obtained solution was detected as described above.

3. Results and discussion

3.1 Characterization of C-dots/NiAl-LDH

The morphology and microstructure of the prepared C-dots, NiAl-LDH and C-dots/NiAl-LDH hybrid material were characterized by TEM. Figure 1a shows the TEM image of C-dots. It demonstrates that the C-dots are spherical and well dispersed. Figure 1b shows the typical TEM image of the NiAl-LDH with platelet nanostructures. The TEM image of the fabricated C-dots/NiAl-LDH hybrid material clearly indicates that the C-dots are assembled on the surface of the NiAl-LDH effectively and dispersedly (Figure 1c and S1† in the Supporting Information). Furthermore, surface charge analysis indicates that the surface charges of C-dots and NiAl-LDH are -5.09 ± 0.5 mV and 3.74 ± 0.3 mV, respectively (Figure S2-S3† in the Supporting

Information). Therefore, C-dots can be attached on the surface of NiAl-LDH through electrostatic attraction. Figure 1d exhibits the corresponding EDX image of C-dots/NiAl-LDH, and the result confirms the presence of Ni and Al elements in the hybrid material.

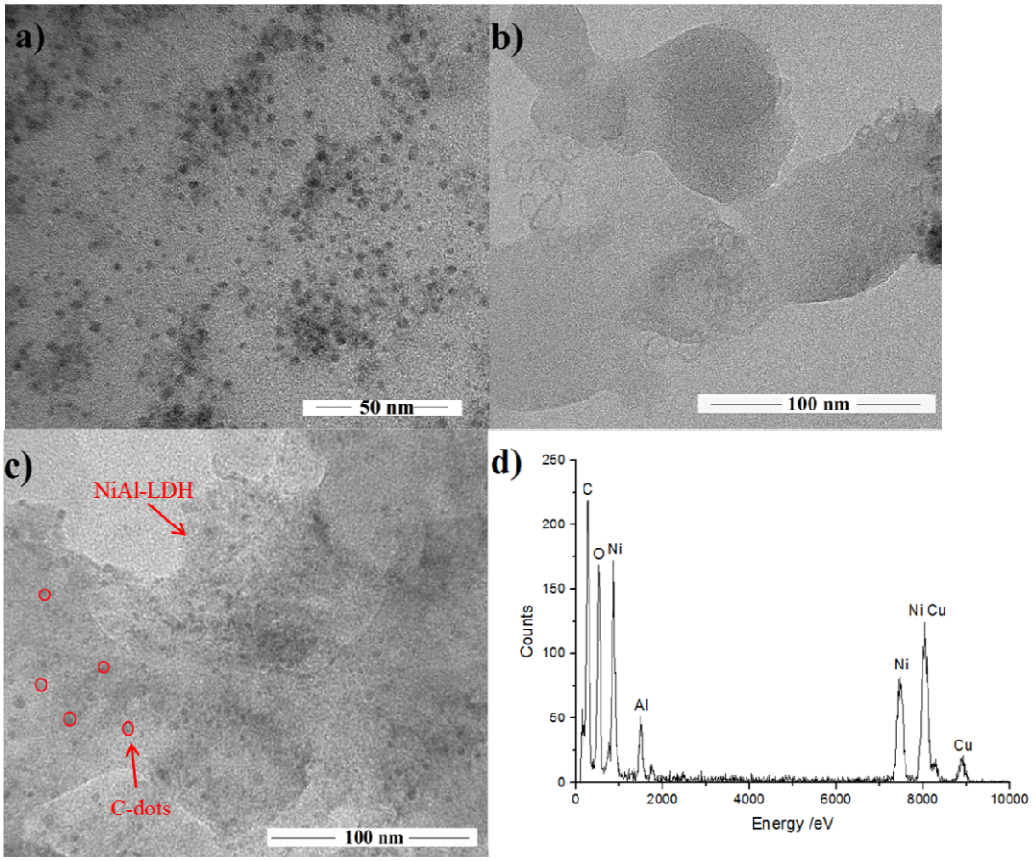

Figure 1. TEM image of (a) C-dots, (b) NiAl-LDH and (c) C-dots/NiAl-LDH composites. (d) EDX pattern of C-dots/NiAl-LDH.

The XRD spectrum of C-dots shows a broad peak centered at around $2\theta=23^{o}$, which is related to the disordered carbon (Figure S4† in the Supporting Information).[36] Figure 2 shows the XRD pattern of NiAl-LDH and C-dots/NiAl-LDH, which exhibits the characteristic reflection of typical hydrotalcite-like structure.[38] Compared with the NiAl-LDH, the intensity of the C-dots/NiAl-LDH diffraction

peaks becomes relatively weak, implying a low crystallinity of the hybrid material.[39] Moreover, the characteristic peak for C-dots at around 23° is too weak to be observed, which may be due to its relatively low diffraction intensity in the hybrid material.[30]

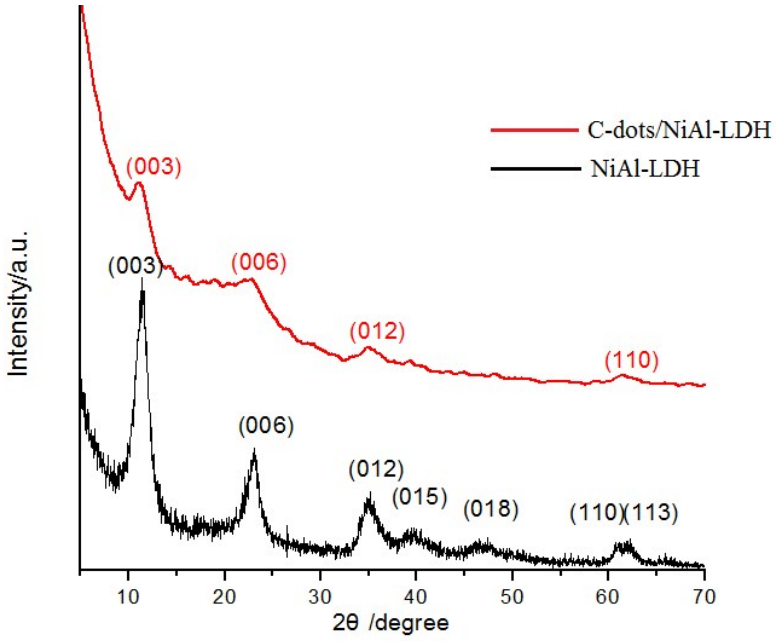

Figure 2. XRD spectra of the NiAl-LDH (black) and C-dots/NiAl-LDH (red) deposited on a glass slide.

In order to obtain more information about the compositions and the surface electronic states of C-dots/NiAl-LDH, the hybrid material was further examined by XPS measurements. Figure 3a displays that the hybrid material is composed of Ni, Al, C and O elements. The high resolution XPS spectrum of C 1s shows that there are still many residual oxygen-containing functional groups on the C-dots surface (Figure 3b).[40] As shown in Figure 3c, the high resolution XPS spectrum of Ni 2p exhibits two major peaks around 856.2 and 873.8 eV, which can assign to the Ni $2p_{3/2}$ and Ni $2p_{1/2}$

levels of Ni^{2+}, respectively.[41] In addition, the high resolution XPS spectrum of Al 2p shows a peak with binding energy of 74.1 eV, indicating the presence of Al^{3+} species in the hybrid material (Figure 3d).[35]

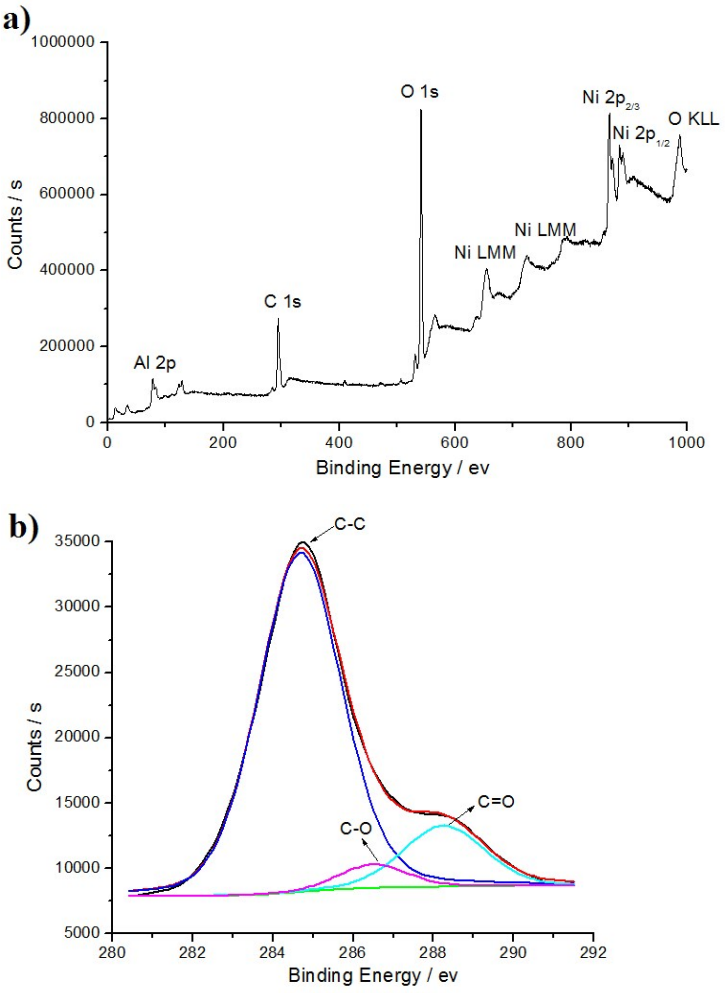

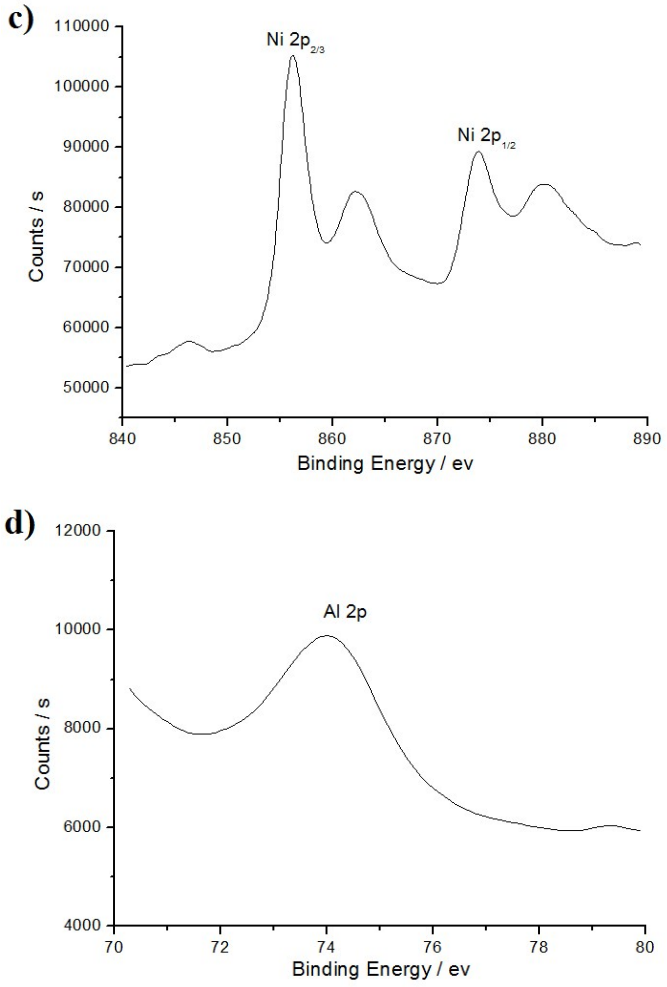

Figure 3. (a) XPS survey spectra of C-dots/NiAl-LDH .and the high-resolution spectra of (b) C 1s, (c) Ni 2p and (d) Al 2p.

The FTIR spectra of C-dots and C-dots/NiAl-LDH are displayed in Figure S5†(see Supporting Information). With respect to pure C-dots, the peaks at about 3429 cm^{-1} can be ascribed to the characteristic absorption bands of the –OH stretching vibration mode. The peaks at 1581 and 1398 cm^{-1} can be attributed to the asymmetric and symmetric stretching vibration of carboxylate (COO^-), respectively.[42-43] The characteristic absorption band of C–H stretching at 2980 cm^{-1} is also observed, and the bands in the range 1000–1400 cm^{-1} implied the existence of C–O groups.[44] In

comparison, the COO^- (1581 cm^{-1}) asymmetric stretching vibration peak of the C-dots/NiAl-LDH is decreased and shifted and the C–O stretching is also decreased, which may be due to the strong electrostatic interactions between the C-dots and NiAl-LDH species.[30]

3.2 Fluorescence properties

Figure 4a shows that the photoluminescence (PL) intensity of C-dots depend on the changes of excitation wavelength, and the maximum intensity region of the C-dots appears at 300-350 nm range in excitation and 420-460 nm range in emission. Figure 4b shows the PL spectra of C-dots, NiAl-LDH and C-dots/NiAl-LDH hybrid material. Compared with C-dots, there is an apparent decay of PL intensity for C-dots/NiAl-LDH. Furthermore, the quantum yield of C-dots/NiAl-LDH (2.3 %) is also lower than that of the C-dots (7.4 %) under the same conditions. Hence, we can conclude that electron transfers exist between C-dots and NiAl-LDH.

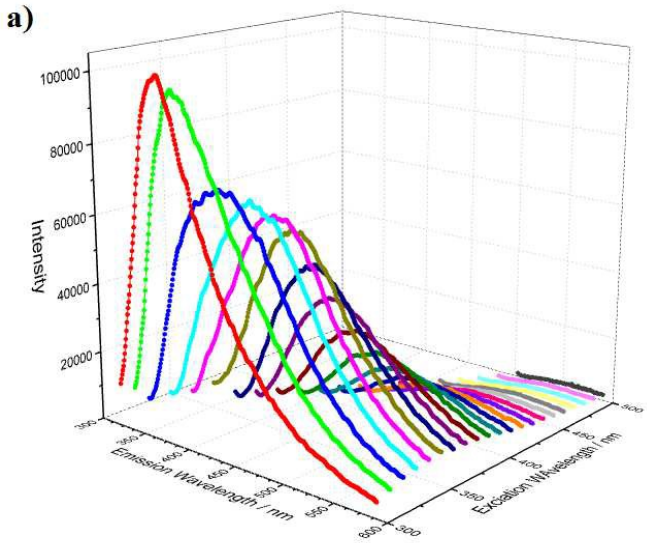

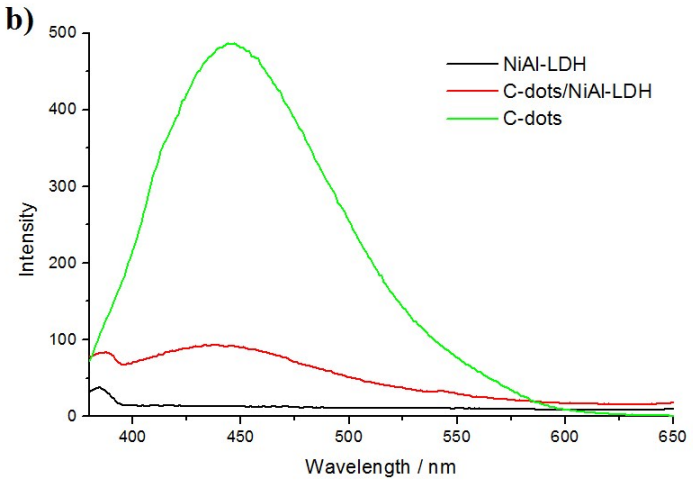

Figure 4. (a) 3D-excitation-emission-intensity spectra of C-dots. (b) PL spectra of C-dots, NiAl-LDH and the C-dots/NiAl-LDH hybrid material (λ_{ex} = 340 nm).

To investigate the fluorescence dynamics of C-dots and C-dots/NiAl-LDH, fluorescence decay traces of C-dots and C-dots/NiAl-LDH are investigated through the single-photon timing technique (Figure 5, Table 1 and Figure S6–S7† in the Supporting Information). The fluorescence decay of C-dots in water displays bi-exponential behavior, and the bi-exponential function (~1.8 ns and ~6.7 ns) is used to fit the decays at all three emission wavelengths. The previous reports have explained that the double de-excitation processes of the C-dots are attributed to a fast band gap transition and long decay of oxygen-related emission.[45-46] Besides, the different emission wavelengths of C-dots do not induce an obvious change in the fluorescence decay.

The fluorescence decay of C-dots/NiAl-LDH also reveals a bi-exponential behavior. The shorter lifetime decreased (~1.8 to ~1.2 ns) along with an increase in the relative amplitude (~43% to ~61%). Moreover, the longer component also decreased (~6.7 to ~5.8 ns) with a decrease in the amplitude (~57% to ~38%). Figure

5 shows that the fluorescence lifetimes of C-dots/NiAl-LDH become shorter as compared with that of C-dots, which may result from the electrons transfer between C-dots and NiAl-LDH quenching the excited state of C-dots.[38] The fluorescence dynamics results are in accordance with the steady-state fluorescence measurements, and the different fluorescence properties between C-dots/NiAl-LDH and C-dots further confirm that C-dots/NiAl-LDH hybrid material is successfully prepared.

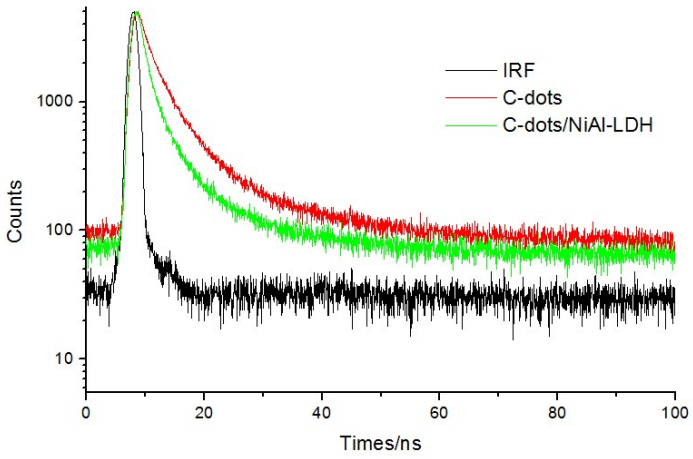

Figure 5. Fluorescence decay profiles (λ_{ex} = 330 nm and λ_{em} = 440 nm) of C-dots and C-dots/NiAl-LDH aqueous suspension.

Table 1 Photophysical properties of C-dots and C-dots/NiAl-LDH aqueous suspension excited at 330 nm. Decay times τ_1, τ_2 and the relative amplitude (%).

Compound	Monitored Emission Wavelength/nm	τ_1/ns	τ_2/ns
C-dots	420	1.66 (42.44 %)	6.48 (57.66%)
	440	1.85 (43.31%)	6.67 (56.69%)
	460	1.98 (42.35%)	6.86 (57.65 %)
C-dots/NiAl-LDH	420	1.20 (60.59 %)	5.61 (39.41%)
	440	1.25 (61.50 %)	5.83 (38.50 %)
	460	1.25 (58.78 %)	6.19 (41.22 %)

3.3 Peroxidase-like activity of C-dots/NiAl-LDH

The peroxidase-like activity of C-dots/NiAl-LDH is evaluated by the catalytic oxidation of TMB in the presence of H_2O_2. As shown in Figure 6, C-dots/NiAl-LDH can catalyze oxidation of TMB to produce a blue product in the presence of H_2O_2. The absorbance peak appeared at 652 nm, which is originated from the oxidation product of TMB (Scheme S1†).[47] In contrast, the experimental condition without C-dots/NiAl-LDH shows negligible color variations. The result indicates that C-dots/NiAl-LDH possesses peroxidase-like catalytic activity. Moreover, control experiment shows that the absorbance of the C-dots/NiAl-LDH system is higher than the C-dots or NiAl-LDH systems, which is probably due to the synergistic effects between C-dots and NiAl-LDH. To further characterize the peroxidase-like activity of C-dots/NiAl-LDH, we repeat the experiments with other chromogenic peroxidase substrates in place of TMB. The C-dots/NiAl-LDH catalyzes the oxidation of different chromogenic substrates, such as ABTS, OPD and DAB display the same color as HRP (Figure S8† in the Supporting Information). All these observations suggest that the C-dots/NiAl-LDH possesses peroxidase-like catalytic activity.

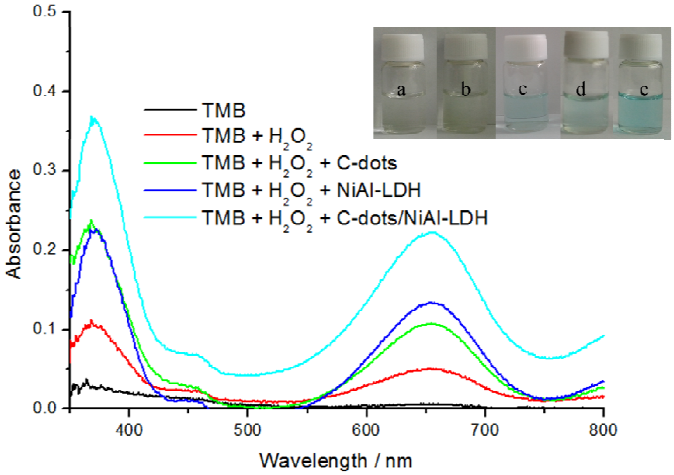

Figure 6. The UV-visible absorption spectra of TMB in different reaction systems:

(a) TMB, (b) TMB + H_2O_2, (c) TMB + H_2O_2 + C-dots, (d) TMB + H_2O_2 + NiAl-LDH and (e) TMB + H_2O_2 + C-dots/NiAl-LDH. Inset: the corresponding photographs of different reaction systems.

Furthermore, the catalytic activity of C-dots/NiAl-LDH is dependent on pH, temperature and the concentration of H_2O_2, which is similar to other nanomaterial-based peroxidase mimics and HRP (Figure 7a-7c). The peroxidase-like activity of the hybrid material is measured by varying the pH from 2.5 to 6, the temperatures from 25 ^oC to 60 ^oC, the H_2O_2 concentration from 0.1mM to 300 mM. Under our experimental conditions, the optimal reaction conditions of C-dots/NiAl-LDH are pH 3.0, 30 ^oC and 20mM (H_2O_2). Based on the above results, C-dots/NiAl-LDH based H_2O_2 detection can be carried out in a relativity wide range of H_2O_2 concentration. A leaching experiment was performed to rule out the possibility that the observed peroxidase-like catalytic activity is caused by leached out Ni^{2+} and Al^{3+}. To perform the leaching experiment, C-dots/NiAl-LDH was incubated in the reaction buffer (pH 3.0) for 10 min and then removed the C-dots/NiAl-LDH nanoparticles from solution by centrifugation. As shown in Figure S9† (see Supporting Information), there is no marked change in the absorbance when the leaching solution was used instead of C-dots/NiAl-LDH nanoparticles under the same reaction conditions. These experimental results reveal that the observed peroxidase-like activity can be attributed to intact nanoparticles.

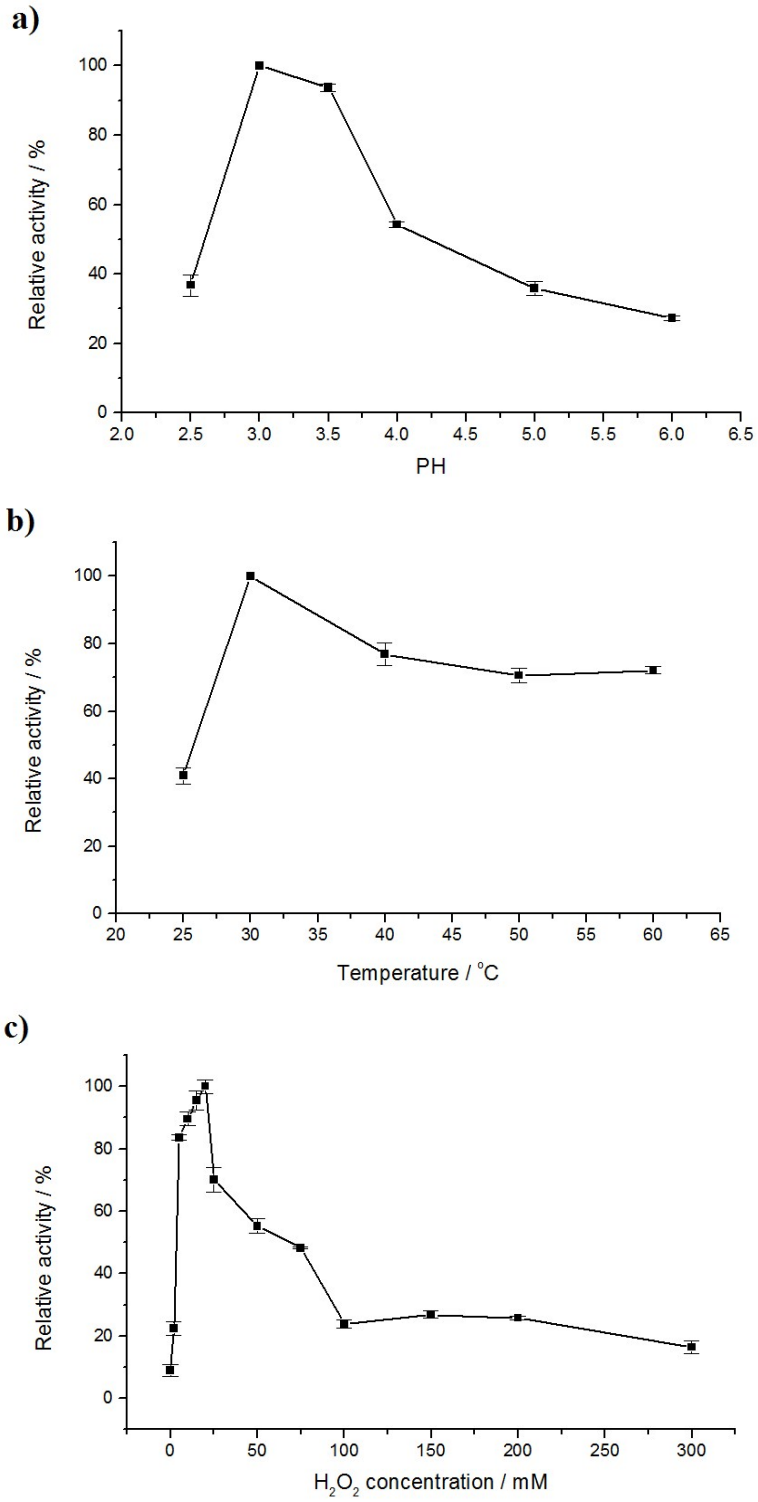

Figure 7. The dependence of the peroxidase-like activity of the C-dots/NiAl-LDH (a) Effect of PH. Conditions: T=30°C, 100 mM H_2O_2. (b) Effect of temperature. Conditions: PH=3.0, 100 mM H_2O_2. (c) Effect of H_2O_2 concentration. Conditions:

PH=3.0, T=30°C. The maximum point in each curve is set as 100%. Error bars represent the standard error derived from three repeated measurements.

To investigate the catalytic mechanism of the C-dots/NiAl-LDH, the steady-state kinetic assays are carried out under the optimal conditions. Typical Michaelis−Menten curves can be obtained in a certain range of TMB or H_2O_2 concentrations (Figure 8). The maximum initial velocity (V_m) and Michaelis–Menten constant (K_m) are calculated from the Lineweaver–Burk plots (Figure 8c-8d and Table S1† in the Supporting Information). The apparent K_m value of C-dots/NiAl-LDH with H_2O_2 as the substrate is higher than that of HRP, which is in agreement with the previous observations that a higher H_2O_2 concentration is required to obtain the maximal activity.[14] On the other hand, the apparent K_m value of C-dots/NiAl-LDH with TMB as the substrate is lower than that of HRP,[2] suggesting that the C-dots/NiAl-LDH has a higher affinity for TMB than HRP. This may be attributed to the larger surface area of the hybrid material and stronger adsorption ability to TMB and higher conductivity of C-dots. In addition, we test the activity of C-dots/NiAl-LDH toward TMB and H_2O_2 under various concentrations, respectively (Figure 8c-8d). It shows that the double-reciprocal plots are almost parallel, revealing a typical ping-pong mechanism.[47] These results indicate that C-dots/NiAl-LDH reacts with the first substrate, and the first product is then released before reacting with the second substrate. The previous reports have pointed out that this product should be a hydroxyl radical (·OH) originated from catalytic decomposition of acidified H_2O_2.[48] Based on the above results, it is believed that C-dots/NiAl-LDH would facilitate the

electron transfer between TMB and H_2O_2 and catalyze the decomposition of H_2O_2 in acidic media into ·OH, which oxidizes TMB to form a blue product. In order to demonstrate the formation of •OH, we then studied the fluorescence changes of terephthalic acid (TA) in the presence of H_2O_2 and C-dots/NiAl-LDH. TA is a highly sensitive and selective fluorescent probe for hydroxyl radicals (•OH).[1] The weakly fluorescent TA can react with •OH and convert into the highly fluorescent 2-hydroxyterephthalic acid (HTA). As shown in Figure S10† (see Supporting Information), the fluorescence intensity of the TA solution is increased with the addition of the C-dots/NiAl-LDH and H_2O_2. The result confirms the production of •OH by the system of H_2O_2 and C-dots/NiAl-LDH.

a)

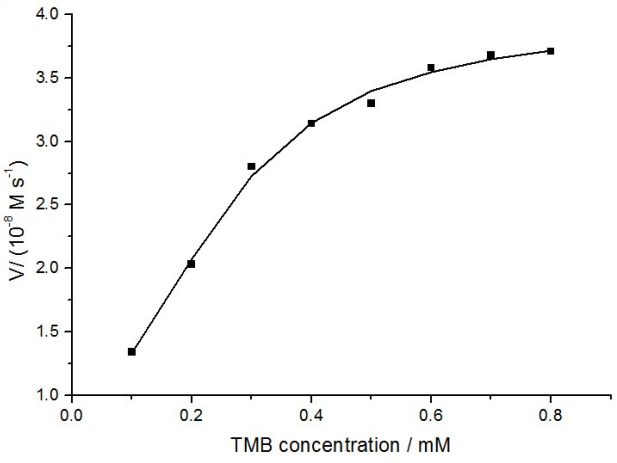

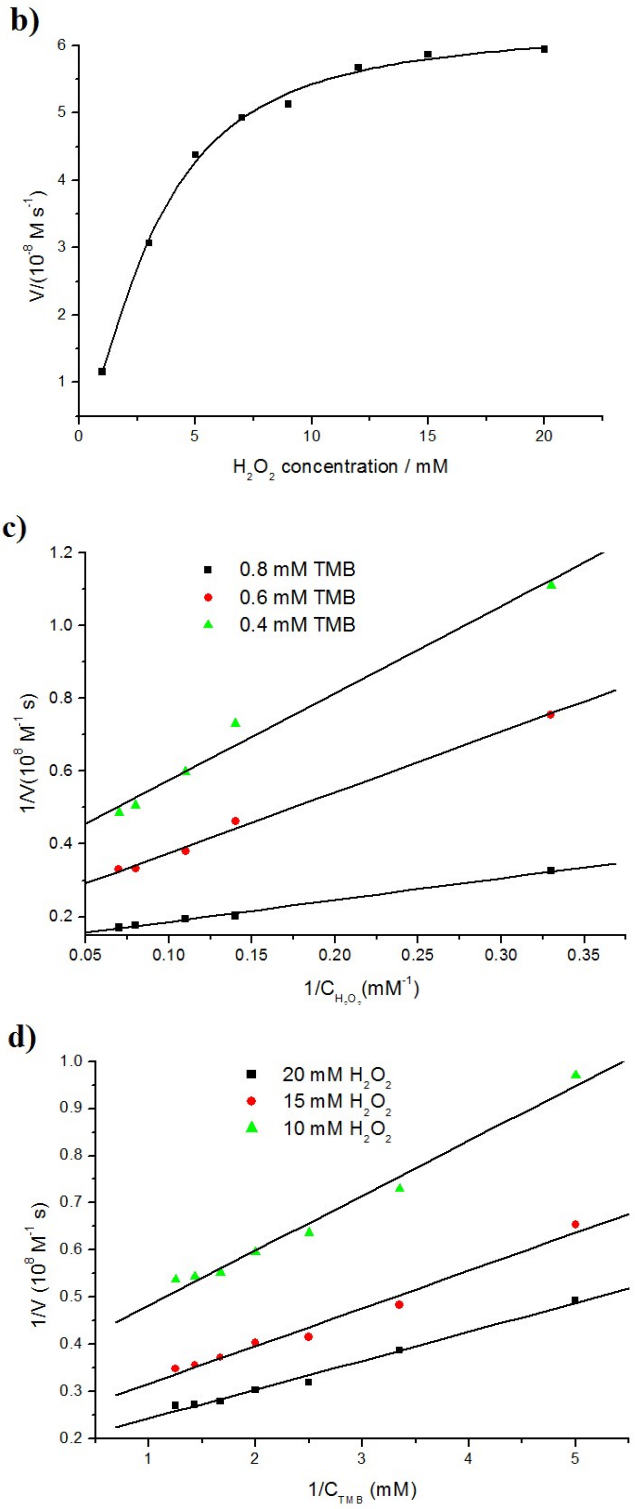

Figure 8. Steady-state kinetic assays of the C-dots/NiAl-LDH (a) The concentration of H_2O_2 was 20 mM and the TMB concentration was varied. (b) The concentration of TMB was 0.8 mM and H_2O_2 concentration was varied. (c, d) Double reciprocal plots

of activity of C-dots/NiAl-LDH with the concentration of one substrate (TMB or H_2O_2) fixed and the other varied.

In general, the activity of natural enzyme is lost after exposing to extreme environment and high temperature.[3] As an inorganic nanomaterial, the C-dots/NiAl-LDH is expect to be more stable than natural enzymes. To verify this, the catalytic activity of C-dots/NiAl-LDH was measured after incubating the hybrid material with different solvents and temperatures for 2 h. The results show that the C-dots/NiAl-LDH hybrid material remains relatively stable after being incubated in different organic solvents, while the HRP loses part of its initial activity (Figure 9a). Moreover, the C-dots/NiAl-LDH hybrid material shows improved thermal stability over a wide temperature range (Figure 9b). The good stability of C-dots/NiAl-LDH hybrid material makes it suitable for a broad range of applications in the biomedicine and environmental chemistry fields.

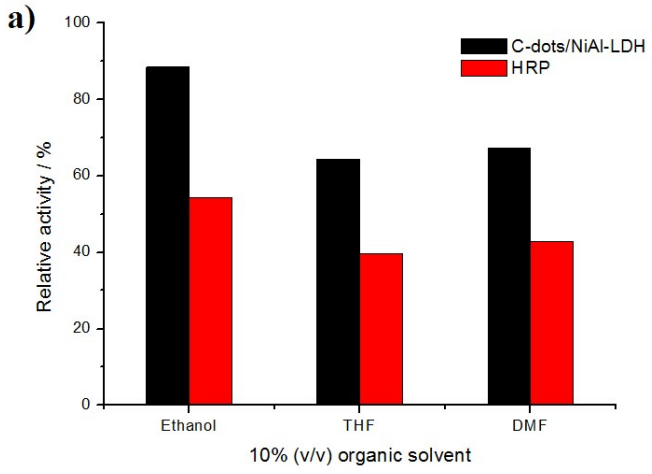

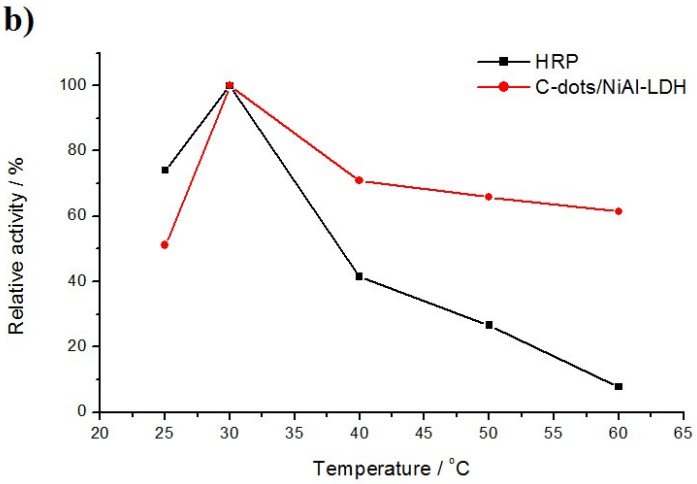

Figure 9. The stability of the C-dots/NiAl-LDH : (a) Activity comparison of C-dots/NiAl-LDH and HRP after exposing to sodium acetate buffer /organic mixed solvents for 2 h at 30℃. (b) Activity comparison of C-dots/NiAl-LDH and HRP after incubating at different temperature for 2 h. The maximum point in each curve is set as 100%.

3.4 Detection of H_2O_2

On the basis of the intrinsic peroxidase-like activity of C-dots/NiAl-LDH, a colorimetric method for detection of H_2O_2 is developed by using the C-dots/NiAl-LDH–TMB–H_2O_2 system. Figure 10a shows a typical H_2O_2 concentration–response curve under optimal conditions. The linear range is from 0.2 to 20 μM (R^2 = 0.9963) with a detection limit of 0.11 μM (Figure 10b). The detection limit is lower than other nanomaterials based-peroxidase mimic, such as gold nanoparticles (0.5μM),[9] CoFe-LDHs (0.4 μM) [15] and CuS-graphene composites (1.2 μM)[17]. This provides a simple, low-cost and convenient colorimetric method for H_2O_2 with high sensitivity.

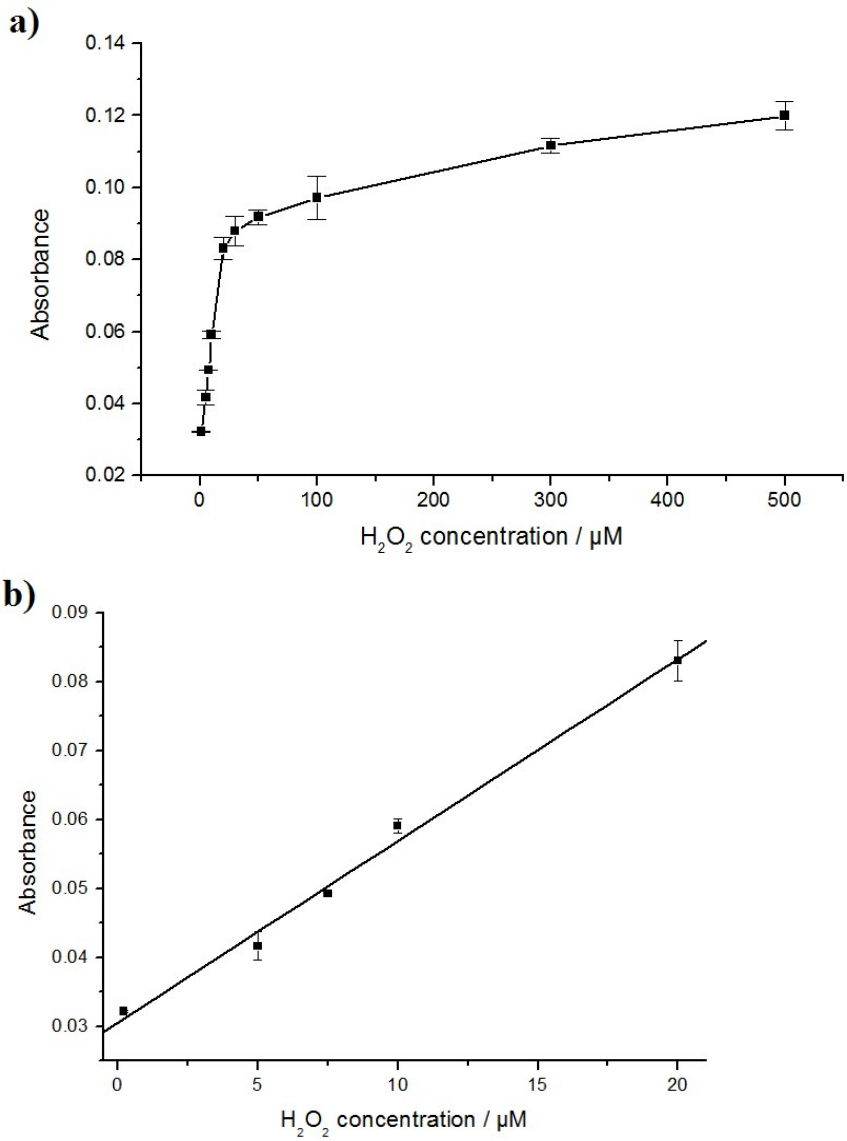

Figure 10. (a) Dependence of the absorbance at 652 nm on the concentration of H_2O_2 from 0.2μM to 500μM. (b) The corresponding linear calibration plot. Error bars represent the standard error derived from three repeated measurements.

As we know, H_2O_2 is the primary chemical for sterilization of plastic packaging material used in aseptic systems. If the subsequent washing and drying process is incomplete, the foodstuff can be contaminated with H_2O_2 residues, which is harmful to human health.[49] Thus, the level of H_2O_2 residues is required to be effectively

controlled within permissible limits. The FDA regulation limits residual H_2O_2 to 0.5 mg L^{-1} in finished food packages.[50] The proposed method based on C-dots/NiAl-LDH-catalyze colorimetric detection is tested in two milk samples for the determination of residues H_2O_2. The two milk samples were aseptic milk and purchased from the local supermarket. According to the calibration curve, the concentration of H_2O_2 is found to be 0.47μM and 0.36μM, respectively, which is lower than the FDA regulation.

4. Conclusion

In summary, C-dots/NiAl-LDH hybrid material has been successfully prepared through the electrostatically self-assembly route. The morphology, structure, composition and fluorescence properties of the hybrid material are studied. Moreover, we have demonstrated that C-dots/NiAl-LDH possesses intrinsic peroxidase-like activity, which can catalyze the oxidation of TMB by H_2O_2 to produce a blue-colored solution. The catalytic activity is dependent on pH, temperature, and H_2O_2 concentration. The kinetic analysis indicates that the catalysis is in accordance with typical Michaelis–Menten kinetics and follows a ping-pong mechanism. Based on the above results, a colorimetric method for the detection of H_2O_2 is developed, and the practical application for H_2O_2 residues analysis in milk samples is performed. The C-dots/NiAl-LDH based colorimetric assay exhibits not only a higher sensitivity for detection H_2O_2, but also a better stability than HRP. Those results suggest that the C-dots/NiAl-LDH hybrid material could be a promising material applied for biochemical analysis.

Acknowledgements

This work was supported by the National Science Foundation for Fostering Talents in Basic Research of the National Natural Science Foundation of China (Grant no. J1103307).The authors would like to thank the Natural Science Foundation of China (no. 21271094).

Notes and references

1 H. L. Tan, C. J. Ma, L. Gao, Q. Li, Y. H. Song, F. G. Xu, T. Wang and L. Wang, *Chem. Eur. J.,* 2014, **20**,16377−16383.

2 L. Gao, J. Zhuang, L. Nie, J. Zhang, Y. Zhang, N.Gu, T. Wang, J. Feng, D. Yang and S. Perrett, *Nat. Nanotechnol.,* 2007, **2**, 577−583.

3 W. Chen, J. Chen, A. L. Liu, L. M. Wang, G. W. Li and X. H. Lin, *ChemCatChem*, 2011, **3**, 1151−1154.

4 X. Liu, Q. Wang, H. Zhao, L. Zhang, Y. Su and Y. Lv, *Analyst*, 2012, **137**, 4552−4558.

5 R. André, F. Natálio, M. Humanes, J. Leppin, K. Heinze, R. Wever, H.-C. Schröder, W. E. G. Müller and W. Tremel, *Adv. Funct. Mater*., 2011, **21**, 501−509.

6 Z. Dai, S. Liu, J. Bao and H. Ju, *Chem. Eur. J*., 2009, **15**, 4321−4326.

7 W. He, H. Jia, X. Li, Y. Lei, J. Li, H. Zhao, L. Mi, L. Zhang and Z. Zheng, *Nanoscale*, 2012, **4**, 3501−3506.

8 T. R. Lin, L. S. Zhong, L. Q. Guo, F. F. Fu and G. N. Guo, *Nanoscale*, 2014, **6**, 11856−11862.

9 Y. Jv, B. X. Li and R. Cao, *Chem. Commun*., 2010, **46**, 8017−8019.

10 H. Jiang, Z. H. Chen, H. Y. Cao and Y. M. Huang, *Analyst*, 2012, **137**, 5560−5564.

11 Y. J. Chen, H. Y. Cao, W. B. Shi, H. Liu and Y. M. Huang, *Chem. Commun*., 2013, **49**, 5013−5015.

12 Y. Song, K. Qu, C. Zhao, J. Ren and X. Qu, Adv. Mater., 2010, 22, 2206−2210.

13 Y. Song, X.H. Wang, C. Zhao, K. Qu, J. Ren and X. Qu, *Chem. -Eur. J*., 2010, **16**, 3617−3621.

14 W. B. Shi, Q. L. Wang, Y. J. Long, Z. L. Cheng, S. H. Chen, H. Z. Zheng and Y. M. Huang, *Chem.Commun*., 2011, **47**, 6695−6697.

15 Y. W. Zhang, J. Q. Tian, S. Liu, L. Wang, X. Y. Qin, W. B. Lu, G. H. Chang, Y. L. Luo, A. M.

Asiri, A. O. Al-Youbi and X. P. Sun, *Analyst*, 2012, **137**, 1325–1328.

16 L. J. Chen, B. Sun, X. D. Wang, F. M. Qiao and S. Y. Ai, *J. Mater. Chem. B*, 2013, **1**, 2268–2274.

17 G. D. Nie, L. Zhang, X. F. Lu, X. J. Bian, W. N. Sun and C. Wang, Dalton Trans., 2013, **42**, 14006–14013.

18 Y. Guo, L. Deng, J. Li, S. Guo, E. Wang and S. Dong, *ACS Nano*, 2011, **5**, 1282– 1290.

19 S. B. He, H. H. Deng, A. L. Liu, G. W. Li, X. H. Lin, W. Chen and X. H. Xia, *ChemCatChem*, 2014, **6**, 1543–1548.

20 Y. M. Dong, J. J. Zhang, P. P. Jiang, G. L. Wang, X. M. Wu, H. Zhao and C. Zhang, *New J. Chem*., 2015, **39**, 4141–4146.

21 G. A. Caravaggio, C. Detellier and Z. Wronski, *J. Mater. Chem*., 2001, **11**, 912–921.

22 G. Abellán, F. Busolo, E. Coronado, C. M. Gastaldo and A. Ribera, J. *Phys. Chem. C*, 2012, **116**, 15756–15764.

23 B. F. Sels, D. E. De Vos and P. A. Jacobs, *Catalysis Reviews*, 2001, **43**, 443–488.

24 S. Navalon, M. Alvaro and H. Garcia, *Appl. Catal., B*, 2010, **99**, 1–26.

25 F. T. Zhang, X. Long, D. W. Zhang, Y. L. Sun, Y. L. Zhou, Y. R. Ma, L. M. Qi and X. X. Zhang, *Sens. Actuators, B*, 2014, **192**, 150–156.

26 L. J. Chen, K. F. Sun, P. P. Li, X. Z. Fan, J. C. Sun and S. Y. Ai, *Nanoscale*, 2013, **5**, 10982–10988.

27 H. T. Li, Z. H. Kang, Y. Liu and S. –T. Lee, *J. Mater. Chem.,* 2012, **22**, 24230-24253.

28 H. T. Li, X. D. He, Z. H. Kang, Y. Liu, J. L. Liu, S. Y. Lian, C. H. A. Tsang, X. B. Yang and S.-T. Lee, *Angew. Chem., Int. Ed.,* 2010, **49**, 4430–4434.

29 S. N. Baker and G. A. Baker, *Angew. Chem., Int. Ed.,* . 2010, **49**, 6726 – 6744.

30 D. Tang, J. Liu, X. Y. Wu, R. H. Liu, X. Han, Y. Z. Han, H. Huang, Y. liu and Z. H. Kang, *ACS Appl. Mater. Interfaces,* 2014, **6**, 7918–7925.

31 Y. L.Wang, Z. C. Wang, Y. P. Rui and M. G. Li, *Biosens. Bioelectron*, 2015, **64**, 57–62.

32 M. L. Zhang, Q. F. Yao, C. Lu, Z. H. Li and W. X. Wang, *ACS Appl. Mater. Interfaces*, 2014, **6**, 20225–20233.

33 J. C. de Mello, H. F. Wittmann and R. H. Friend, *Adv. Mater.,* 1997, **9**, 230–232.

34 Q.Y. Liu, G. L. Fan, S.Y. Zhang, Y.C. Liu, F. Li, *Mater. Lett*., 2012, **82**, 4–6.

35 H. Wang, X. Xiang and F. Li, *J. Mater. Chem*., 2010, **20**, 3944–3952.

36 Y. L. Guo, D. Wang, X. Y. Liu, X. D. Wang, W. S. Liu and W. W. Qin, *New J. Chem*., 2014, **38**, 5861–5867.

37 Y. L. Guo, X. Y. Liu, C. D. Yang, X. D. Wang, D. Wang, A. Iqbal, W. S. Liu and W. W. Qin, *ChemCatChem*, 2015, **7**, 2467-2474.

38 Q.Y. Liu, G. L. Fan, S.Y. Zhang, Y.C. Liu, F. Li, *Mater. Lett*., 2012, **82**, 4–6.

39 J. Yang, C. Yu, X. M. Fan, Z. Ling, J. S. Qiu and Y. Gogotsi, *J. Mater. Chem. A*, 2013, **1**, 1963–1968.

40 D. Tang, Y. Z. Han, W. B. Ji, S. Qiao, X. Zhou, R. H. Liu, X. Han, H. Huang, Y. Liu and Z. H. Kang, *Dalton Trans*., 2014, **43**, 15119–15125.

41 J. W. Lee, T. Ahn, D. Soundararajan, J. M. Ko and J. D. Kim, *Chem. Commun*., 2011, **47**, 6305–6307.

42 W. B. Lu, X. Y. Qin, S. Liu, G. H. Chang, Y. W. Zhang, Y. L. Luo, A. M. Asiri, A. O. Al-Youbi and X. P. Sun, *Anal.Chem.*, 2012, **84**, 5351–5357.

43 L. Zhou, Y. H. Lin, Z. Z. Huang, J. S. Ren and X. G. Qu, *Chem. Commun.,* 2012, **48**, 1147-1149.

44 X. F. Jia, J. Li and E. K. Wang, *Nanoscale*, 2012, **4**, 5572–5575.

45 M. Y. Chen, W. Z. Wang and X. P. Wu, *J. Mater. Chem. B*, 2014, **2**, 3937–3945.

46 L. Bao, Z. L. Zhang, Z. Q. Tian, L. Zhang, C. Liu, Y. Lin, B. P. Qi and D. W. Pang, *Adv. Mater*., 2011, **23**, 5801–5806.

47 X. Jiang, C. J. Sun, Y. Guo, G. J. Nie and L. Xu, *Biosens. Bioelectron*., 2015, **64**, 165–170.

48 M. L. Zhang, Q. F. Yao, W. J. Guan, C. Lu and J. –M. Lin, *J. Phys. Chem. C,* 2014, **118**, 10441–10447.

49 J. F. Ping, X. L. Mao, K. Fan, D. Y. Li, S. P. Ru, J. Wu and Y. B. Ying, *Ionics*, 2010, **16**, 523-527.

50 M.E. Abbas, W. Luo, L. H. Zhu, J. Zou and H. Q. Tang, *Food chem.*, 2010, **120**, 327-331.